Crack quasi-healing in films of vertically aligned 1D nanostructures: Impact of compliance in a 1D geometry

Ludovic Pauchard, Frédérique Giorgiutti-Dauphiné, David Mcilroy

Crack quasi-healing in films of vertically aligned 1D nanostructures: impact of compliance in a 1D geometry

Ludovic Pauchard,[1] Frédérique Giorgiutti-Dauphiné,[2] and David McIlroy[3]
[1)] *Université Paris-Saclay, CNRS, FAST, 91405, Orsay, France*
[2)] *Université Paris-Saclay, CNRS, FAST, 91405, Orsay, France*
[3)] *Oklahoma State University - Stillwater, USA*

(*Electronic mail: ludovic.pauchard@universite-paris-saclay.fr.)

(Dated: 17 March 2022)

We study nanostructured films made of helical nanowires, nanosprings, which provide remarkable mechanical behaviour. When subjected to wetting and drying processes, these films crack like most coatings. However, beyond the great ability of these films to shrink, the cracks partially close when these films are no longer mechanically stressed. While for conventional coatings about 20% of the crack opening is relieved, more than 80% of the crack opening is relieved in films of nanosprings when the film is unloaded. We show here that this quasi-reversibility is related to (i) the high compliance of the material, (ii) the low energy consumed by plasticity, and (iii) the high deformability of the film components, e.g. the nanosprings. These results are compared to the case of usual particulate films.

I. INTRODUCTION

Nanostructured materials have attracted considerable attention in both academic and industrial circles in the past decade due to their potential applications in fields such as chemical sensors[1,2], as well as optoelectronic devices[3,4]. In particular, they exhibit widely adjustable mechanical properties, which provide promising applications in biointerface materials that can guide the design of synthetic materials for tissue engineering and healing. Among the emerging group of nanostructures, helical nanowires, e.g. nanosprings, are multiple functional nanomaterials[5,6]. A key question concerning these materials is how failures develop. In this context, we address the formation of cracks in successively stressed compliant nanospring films. In general, crack patterns depend on the applied stress and the way the material releases it. The cracks thus present geometrical characteristics described by the following parameters: depth, thickness, density, spacing, and aperture. In this way, the crack pattern reveals the mechanical properties of the material[7] and offers a wide variety of applications[8,9]. These patterns have been extensively observed in a variety of materials, such as ceramics, paints or particulate coatings where cracking results from solvent evaporation[10–15]. In the last, capillary forces produced by the surface tension of the solvent are sustained by the wet structure. Therefore, the mechanical response of the structure determines the ability of the material to release the stress through significant overall shrinkage or cracking. For particulate coatings, after drying is complete, cracks close to less than 20% of their initial opening or remain opened which attest to plastic behaviour.

In this article, we consider here films of Vertically-Aligned NanoSprings, e.g. VANS, that is a highly porous material bonded to a stiff substrate. The formation of cracks in these nanostructured films shows specific characteristics compared to conventional brittle coatings such as colloidal coatings. Indeed, these compliant films that are stressed by wetting and drying present a high ability to shrink. The resulting cracks exhibit a large opening, then close over more than 80% of their initial opening when the film is unloaded (figure 1). This quasi-healing is due to several characteristics as evidenced in this article. On the scale of the film, the compliance of the film has been highlighted through nanoindentation testing. Moreover, considerations based on an energy balance provide an estimation for the weak energy plastically consumed in the films during the opening/closing of the cracks. This points out the remarkable dominance of film elasticity. On the scale of film components, the high deformability of the individual nanosprings is supported by their flexible and elongated shape. Moreover, the mechanical stability of the films has been highlighted through cyclic loading and repeated wetting/drying processes. These physical properties are significantly different from those of the usual particulate materials. These results support the idea that VANS have extraordinary mechanical properties, hence are a particularly promising system for biomimetics. utilizing a combination of nanospring coating with specific materials.

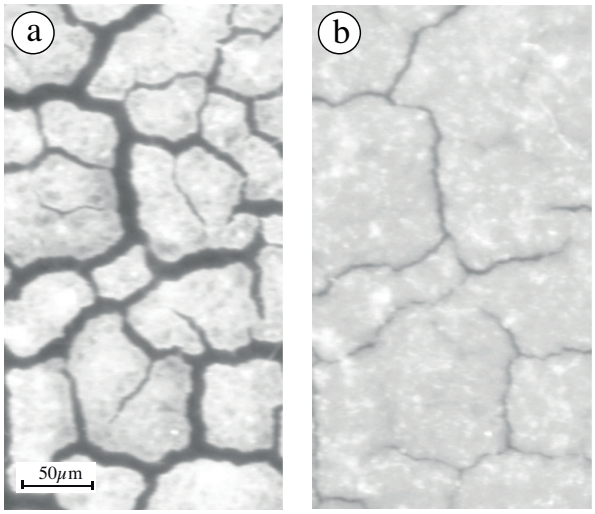

FIG. 1. Drying-induced cracks: maximal crack opening (a) then closure (b). Some cracks heal completely at the microscopic scale.

II. EXPERIMENTAL

A. Nanosprings synthesis

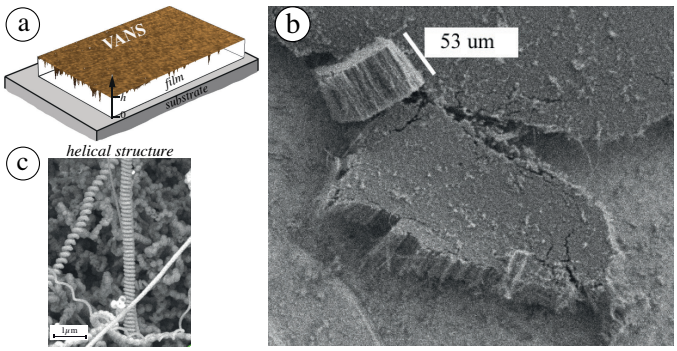

FIG. 2. (a) A schematic representation of a film of Vertically-Aligned NanoSprings (VANS) on a *Si* substrate. (b) Scanning Electron Microscopy micrographs of a film of VANS and (c) individual nanosprings.

The nanospring film consists of an array of helical silica nanowires aligned perpendicularly to the substrate surface, e.g. Vertically-Aligned NanoSprings (VANS), as shown in figure 2a,b. We synthesize the helical nanowires via a modified Vapor-Liquid-Solid (VLS) mechanism on a *Si* substrate. A detailed description of the nanospring growth process can be found in references by McIlroy et al.[16] and Wang et al.[6]. The highly dense array of nanosprings is due to the density of particles sputtered onto the *Si* substrate and serving as the catalyst for the VLS process. The areal density is estimated at $m = 5 \times 10^{10}$ nanosprings per cm^2 using SEM micrographs[17]. In turn, the helical nanowires growth uses catalytic liquid droplets at the tip of the nanowires. The catalytic particle adsorbs the molecules of the vapour and then diffuse towards the particle-nanostructure interface. A controlled asymmetry leading to an anisotropy in the contact angle at the catalyst droplet-nanowire interface is responsible for a torque of the droplet[5]. This process results in the formation of a helical structure. The thickness of the nanospring film was varied by controlling the growth rate of the nanospring on the substrate. In this way, the measurements are carried out on films with a thickness of 8μm, 14μm and 26μm. The cohesion of the vertically aligned nanosprings in the film is ensured by chemical bonding SiO_x-SiO_2, x=1-2[18]. Hence the order of magnitude of the surface energy for VANS in the air is estimated to be $0.5 J/m^2$. This results in a structural coating.

B. Mechanical properties characterization

1. *Global elastic response*

The mechanical response of the nanospring films is examined using nanoindentation testing (Anton-Paar). The method consists of driving a spherical tip into the sample with a controlled force, F (see the sketch in figure 3a). The range of

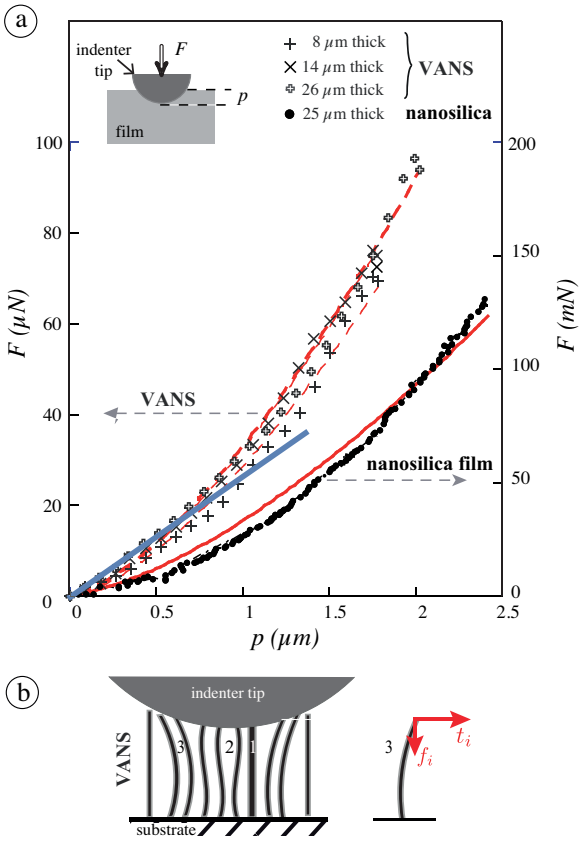

FIG. 3. Mechanical behaviour using indentation testing. (a) The load, F, applied to materials is plotted as a function of the penetration depth, p, of the indenter tip. Measurements were carried out on VANS exhibiting three film thicknesses (8, 14 and 26μm) and on a silica film (LUDOX - HS40) 25μm thick. The red lines are the theoretical predictions in accordance with the Hertz contact law. The blue line is the theoretical predictions in accordance with equation 2 for VANS. (b) Schematics of consecutive contacts of the indenter tip and nanosprings: bending deflection at the tip of the nanospring i resulting from indentation force f_i and lateral force t_i. Different events can take place: compression (1), buckling (2), bending under the effect of the forces in red (3) (the bonds between wires are not illustrated).

applying loads lies from $\sim 1\mu$N up to 100μN. The spherical tip of radius $R = 200\mu$m assumed to be perfectly rigid is initially in contact with the surface of the film. Then the tip is driven inside the sample with a controlled loading speed of 100mN/min until a maximum load is reached.

The standard procedure of Oliver and Pharr[19] to estimate the elastic modulus from the indentation load-displacement curve uses the initial slope of the unloading curve upon unloading as the material recovers elastically (see figure 4 of the Supplementary Material). In the following we measure the elastic behaviour of the material due to a axial compression using the following process. The applied force is measured as a function of the penetration depth, p, of the indenter tip in the material. This method is a way to extract the average value of the elastic modulus, E, of the coating. Measurements are reported in figure 3a for films of VANS at various thicknesses.

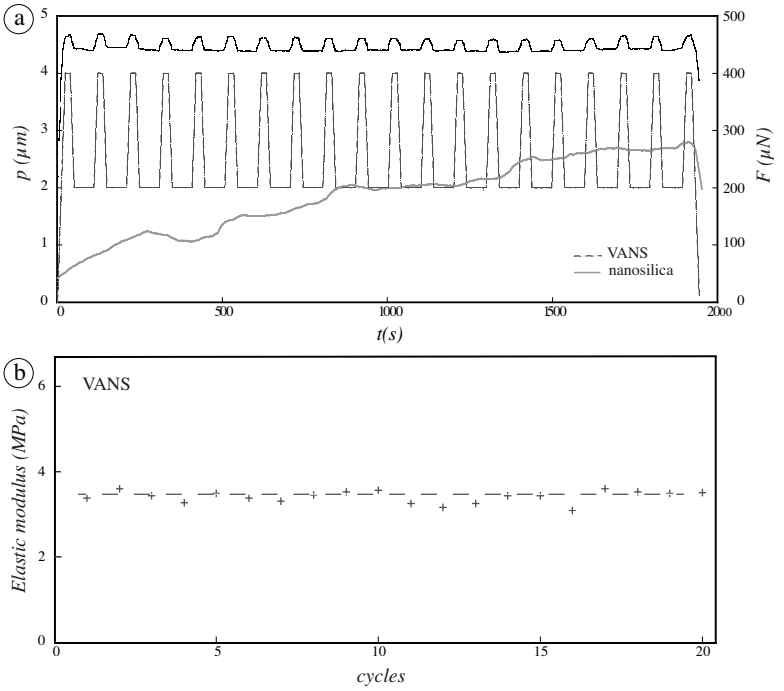

FIG. 4. (a) Time dependence of the indentation depth, p, under a cyclic indentation load, F, for a nanospring film, 26μm thick, and for a film made of nanosilica particles (LUDOX - HS40, $\sim 25\mu$m thick). (b) The resulting elastic moduli are plotted following each load/unload cycle for the nanospring film. The elastic moduli are estimated using the standard Oliver and Pharr procedure[19] (see Supplementary Material). The dashed line is a guide for the eyes.

The loading curves are well fitted by the Hertz contact law revealing the elastic behaviour of the material due to a axial compression:

$$F = \frac{4\sqrt{R}}{3(1-\nu^2)} E p^{3/2}, \quad (1)$$

where ν is the Poisson's ratio of the film. This technique provides measurements of the film's compressive axial stiffness but does not take into account the anisotropy of the mechanical properties of the helical structure: the stiffness was found to be $4-5$ times larger in the vertical direction than in the horizontal one[20]. Thus, the average value of the vertical stiffness of the nanospring films is estimated to be $E_{VANS} = 2.34 \pm 0.18$ MPa based on the curve fitting using equation 1 ($\nu = 0.27$[21]). This low value indicates that the nanospring films exhibit compliant properties, where minor stress is required for a considerable strain. Note that the film thickness barely influences the measurements.

The stiffness of the nanospring films is compared to that of a particulate coating: in particular, the drying of dispersions of charged silica nanoparticles (LUDOX - HS40 commercially available from Sigma-Aldrich with a particle size of 12μm) leads to solid films whose stiffness, E_{silica}, is obtained using microindentation testing (CSM Instruments Micro Indentation Tester, MHT with a range of applying loads lies from ~ 20 mN up to 10 N) as shown in figure 3a. The loading curve fitted using the Hertz contact law gives $E_{silica} = 1.5 \pm 0.3$ GPa (using $\nu = 0.18$[22]).

Besides, the reproducibility of the mechanical response was analyzed through repeated indentation tests as shown in figure 4a. In the case of nanospring films, the cyclic loading between loaded 400μN and unloaded states 200μN results in a cyclic penetration depth at a loading rate of 1000μN/min . No changes in the average indentation depth are captured in each indentation cycle: the cyclic loading results in a cyclic penetration depth at a constant load repetition. This mechanical response of the film is only observed when the delay between load/unload cycles is not too short ($> 5s$), in which case the average penetration depth into the material monotonously increases during the cycles (see Supplementary Material). The mechanical response of the nanospring film is changed with loading frequency, suggesting a relaxation process of the individual nanosprings.

However, in the case of the particulate coating, the penetration depth monotonously increases during the cyclic indentation load which underlines the inelastic characteristics of the particulate film under repeated loading. These results on nanosilica films are consistent with measurements obtained in other particulate films made of different silica particles as well as stiff latex particles. The resulting elastic moduli are reported in figure 4b as a function of the number of cycles. Here we use the standard procedure of Oliver and Pharr[19] to estimate the elastic modulus as the material recovers elastically at the beginning of the unloading process.
Hence, these results confirm the mechanical stability of nanospring films under repeated loading.

2. Individual elastic contribution of nanospring

The above investigations allow us to obtain the global elastic response of nanospring films. However, the results do not account for the individual elastic contribution of nanosprings. In this way, the following considerations are carried out to estimate the stiffness of individual nanosprings. The mechanical response of nanospring films involves different processes such as axial compression, buckling or bending of nanosprings as sketched in figure 3b. This was particularly investigated in the case of a forest of pillars in reference[23]. In the case of nanospring films, no changes characterizing the transition between compression and buckling of nanosprings can be captured apart from indentation curves in figure 3a. Moreover, since axial compression rapidly requires a significant amount of elastic energy during the loading process, the buckling or bending process preferentially contribute to the deformation of the film. Assuming that bending is the most likely deformation due to the lateral forces, t_i, acting on nanosprings (figure 3b), the total indentation force, F, can be related to the stiffness of individual nanosprings, $\mathscr{E}$, through the classical nonlinear beam theory. By integration over the contact area A between the indenter and the film, it comes[23]:

$$F = \int_A \frac{\pi^2 \mathscr{E}}{4h^2} m\Big(1 - \frac{1}{(1+(p-p_i)R^2/(h.r_i^2))^{1.15}}\Big) dA_i, \quad (2)$$

where h is the nanospring length (film thickness), p_i is the indentation depth of the nanospring i at a distance r_i from the axis of symmetry of the indenter and $dA_i = 2\pi R dh_i - 2\pi r_i dh_i$.

Considering $h = 26\mu$m, the curve fitting by equation 2 at low penetration depth, p, gives $\mathscr{E} = 0.20 \pm 0.04$TPa (figure 3a). The last value is close to the order of magnitude obtained in reference[20]. Note that this value is barely modified if we consider the case of buckling of the nanosprings instead of bending.

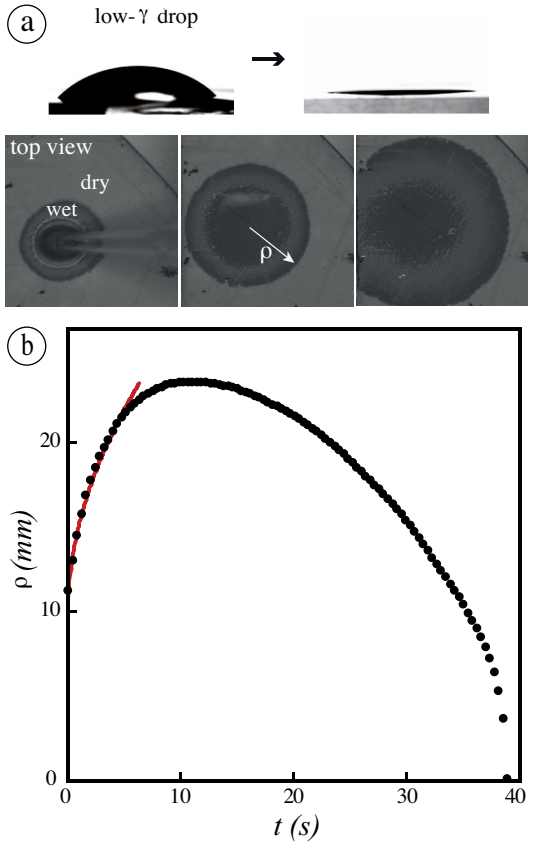

FIG. 5. (a) Wetting on a film of nanosprings. Deposition / spreading / imbibition of a drop of a low-surface-tension solvent (ethanol) into VANS (side and successive top views). (b) The radius, ρ, of the wetted region is plotted as a function of time: the time increase of ρ corresponds to the imbibition process (the line is the best fit using equation 3), while the time decrease of ρ is characteristic of the evaporation of the solvent.

III. RESULTS AND DISCUSSION

A. Wetting films of nanospring

An important specificity of nanospring films lies in the high porosity of the system[24]. To capture the permeability of the system, the process of drop imbibition in the film has been carried out. When a water drop is deposited on the surface of the nanospring surface, the drop keeps a spheroidal shape due to the air pockets trapped underneath (see figure 5 in the Supplementary Material). However, a droplet of a low surface tension liquid (ethanol) spreads and rapidly soaks into the nanospring film (figure 5a). Measuring the time variation of the drop imbibition is a simple way to estimate the voids size, a, between the nanosprings. In general, the fluid flow through nanoporous materials can be described by the Washburn equation that enables to obtain the time variation of the radius, $\rho(t)$, of the wetted region as[25]:

$$\rho(t) = (\gamma_{lv}.a.\cos(\theta)/(2\eta))^{1/2}\sqrt{t}, \quad (3)$$

where γ_{lv} is the liquid-vapor interfacial tension, η its viscosity and θ the contact angle of the liquid with the solid material.

The adjustment of the measurements with equation 3 at the first moments of the imbibition process allows us to obtain an order of magnitude of the voids size of about one hundred nanometers (figure 5b). These experiments were reproduced on 3 films of different thicknesses as reported in Table I.

	VANS		
film thickness h (μm)	8	14	26
effective size a (nm)	95±15	118±12	110±9

TABLE I. Order of magnitude of the voids size estimated by the measurements of liquid imbibition in nanospring films (VANS). 3 film thicknesses have been considered.

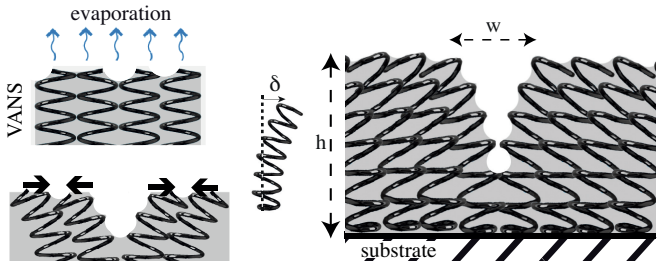

FIG. 6. Drying. Sketch in side view illustrating the crack opening induced by capillary shrinkage. Deflection δ of a single nanospring. Crack opening, w, in a network of nanosprings.

B. Cracks induced by drying of wetted nanospring films

Evaporation of the volatile liquid from a wet porous film generally results in the formation of cracks. Cracking is caused by strong capillary forces assisted by the inherent elasticity of the film. In this way, evaporation forms pinned menisci at the liquid-vapour interface. The surface tension of the solvent causes a pressure difference, $\Delta\mathscr{P}$, at the evaporation surface with respect to the vapour pressure (figure 6). According to the Young-Laplace equation this pressure difference expresses as: $\Delta\mathscr{P} = \frac{2\gamma_v \cos(\theta)}{\mathscr{R}}$, where $\mathscr{R}$ is the radius of curvature of the menisci. As a result, the capillary pressure causes the network of nanosprings to collapse and the film to shrink at the evaporation surface[24,26]. The shrinkage is related to the nanosprings deflection whose displacement, δ, is determined by:

$$\delta = \frac{\mathscr{F} h^3}{8\mathscr{E} I}, \tag{4}$$

where $\mathscr{F} = \Delta\mathscr{P}.h.d$ is the capillary force acting on the nanosprings and $I = \pi d^4/64$ is the cross-sectional second moment of a single nanospring assimilated to a wire of diameter d. The deflection results in the aggregation of the wires[27].
This mechanism results in the aperture of the film that scales as $w \sim 2\delta$ as sketched in figure 6. Considering an average diameter $d = 10$nm of a $h = 26\mu$m long nanospring and elastic modulus $\mathscr{E} = 0.20 \pm 0.04$TPa, the capillary pressure associated with $\mathscr{R} \sim w$ is estimated at $3k$Pa leading to a film aperture of 25μm which is consistent with the measurements from images in figure 1 and figures 8. This process governs the formation of cracks in the film (figure 8). The cracks invade the plane of the film to release the residual stress. Hence, crack formation is governed by the combination of three classical processes:

- nucleation: cracks nucleate at some defects (figure 8b);
- crack opening;
- propagation. The cracks do not form simultaneously but provide a degree of hierarchy: this is particularly the case in figure 1 where the first crack to form are wider than the second and the third generation[28].

Finally, the morphology of cracks shows a partial branched network whose topology is characterized by junctions and dead ends (figure 8a).

At final stage of the drying, the film is unloaded and the capillary force $\mathscr{F}$ the force is reduced to 0. As a result, the deflection is cancelled and the cracks close up.

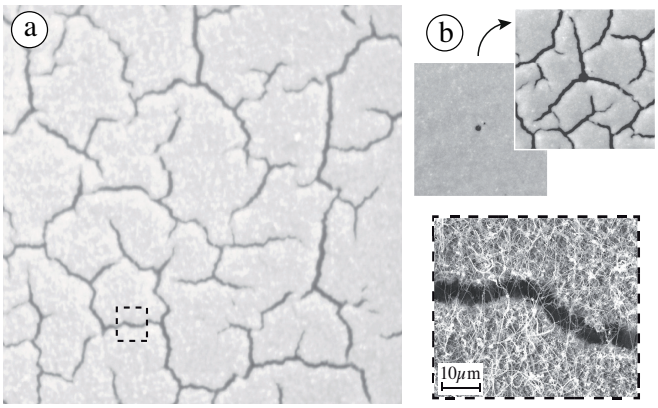

FIG. 7. (a) Branched network of cracks induced by drying a wet film of nanosprings (image width $= 500\mu$m; film thickness $= 26\mu$m); a Scanning Electron Microscopy micrograph is shown in the dashed square. (b) Star-like patterns with 3-branched cracks nucleated from a nucleation site.

These features are commonly encountered in the formation of cracks induced by the drying of particulate films: the shrinkage at the drying face is constrained by the adhesion of the film to the substrate. As a result, differential shrinkage is governed by the variation of liquid pressure in the pores and results from a stress distribution within the film. In the following we focus on the crack aperture.

C. The impact of compliance on crack quasi-healing in nanospring films

The time variation of the crack opening then closure induced by a wetting/drying process is reported in figure 8 . The crack opening strongly evolves during the drying process as shown in figure 9a. The measurements of the crack opening, w, are correlated to the time variation of the evaporation rate, V_D, which is deducted from the film mass variation with time during the drying (figure 9b); $t_D = h/V_D$ corresponds to the drying timescale. In the first stage, the crack widens during a drying period characterized by a constant evaporation rate. This holds for brittle colloidal films, as shown in the plot corresponding to a nanosilica film in figure 9a. Crack opening results from the build-up of the drying stress in the porous film[29]. Thus, the dynamics of the crack opening appears to be well-controlled by the drying process. The crack opening stops at a maximum value (image 1 for VANS in figure 9). This maximum value is related to the mechanical properties of the film[29] and appears to be much higher in the case of VANS than in the case of common particulate materials. This reveals a much greater capacity for shrinkage for nanosprings than for nanoparticle gels. At a point, the drying process ceases, which

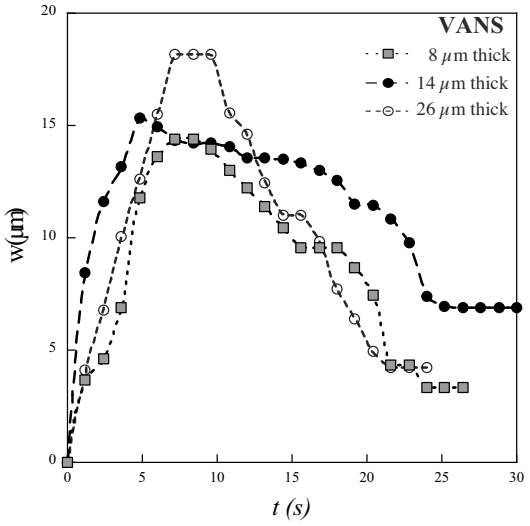

FIG. 8. Time variation of the crack opening then closure induced by a wetting/drying process. Three film thicknesses are shown.

is highlighted by the jump of the evaporation rate, as shown in figure 9b. As the liquid located within the porous structure evaporates, the pores become empty modifying the refractive index of the film (as evidenced by the change in the shade of grey in images 1 and 2 in figure 9). The consequence of the sudden decrease for the evaporation rate is that the tensile drying stress vanishes and cracks close up as a result of the elastic response of the film (image 2 and 3 in figure 9). At the final stage, the crack opening is noted w_p.

Whether or not the closure is complete, we observe, on average, that more than 80% of the crack opening is reversible for VANS, while less than 20% of the crack opening is relieved for usual brittle coatings. Indeed, the ratio between the maximum value of the crack opening and the reversible part of the crack displacement, $w-w_p$, is shown in figure 10 for a variety of films. The different materials are presented by their compliance defined as $C=E^{-1}$ that attests to the ability of deformation. In general, the irreversibility of the crack closure results from the plastic deformation of the material. The following considerations, based on an energy balance, compare the energy plastically consumed in VANS and in nanosilica coatings through the measurements of the crack opening/closure. In pure tensile loading the crack opening may be written as:

$$w \sim \frac{K_c}{E} l^{1/2} \tag{5}$$

where l is the distance along the crack from its tip and K_c is the critical stress intensity factor that designates the minimum stress intensity required to get an existing crack to propagate[30]: $K_c=\sqrt{G_c E}$, where G_c is the energy release rate. The energy balance states that the energy release rate is the sum of the work (or surface energy), W, used to create the new crack surfaces and the irreversible energy, U_p due to plastic losses. The reversible part of the crack displacement, $w-w_p$, involves the reversible work W used to create the new

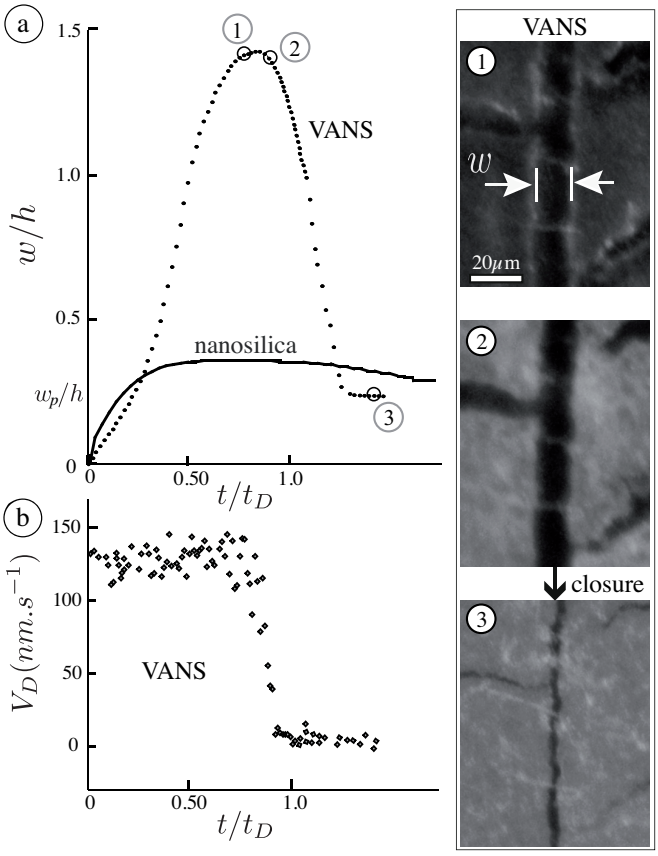

FIG. 9. (a) Typical crack opening and closing induced by the drying of wet films. The time variation of the crack opening, w, over the film thickness, h, is reported in the case of VANS (dots) and a nanosilica film (plain line); t_D is the drying timescale which is proportional to the film thickness. Measurements were performed on the same crack. In the case of VANS, the film, 26μm thick, is wetted by surfactant-enhanced water. The value of the opening when the drying process ceases is noted w_p. The corresponding images of a crack in VANS are referred as $1,2,3$. (b) Time variation of the drying rate, V_D, deduced from mass variation with time of a wet film of VANS.

surfaces in an ideal material without plastic losses ($U_p=0$). Thus equation 5 gives the ratio between the crack opening and the reversible part of the crack displacement as follows:

$$w/(w-w_p) = (1+U_p/W)^{1/2} \tag{6}$$

A similar equation was obtained by Goehring et al.[14]. Note that this analysis assumes that a crack is opening in a uniform material with uniform field tensile stress.

The order of magnitude of the surface energy for nanosilica films, W^{silica}, is estimated to be twice the surface tension of the solvent (water) for the nanosilica films: $\sim 0.14 J/m^2$[11] while for VANS $W^{VANS} \sim 0.5 J/m^2$ for VANS[18]. Hence, the measurements reported in figure 10 together with the equation 6 allows one to estimate the irreversible energy consumed during the opening/closure of drying cracks in VANS, $U_p^{VANS} = 0.05 \pm 0.01 J/m^2$, much lower than that for typical nanosilica films, $U_p^{silica} = 4.0 \pm 0.5 J/m^2$.

Among the different origins of plasticity in the nanosprings

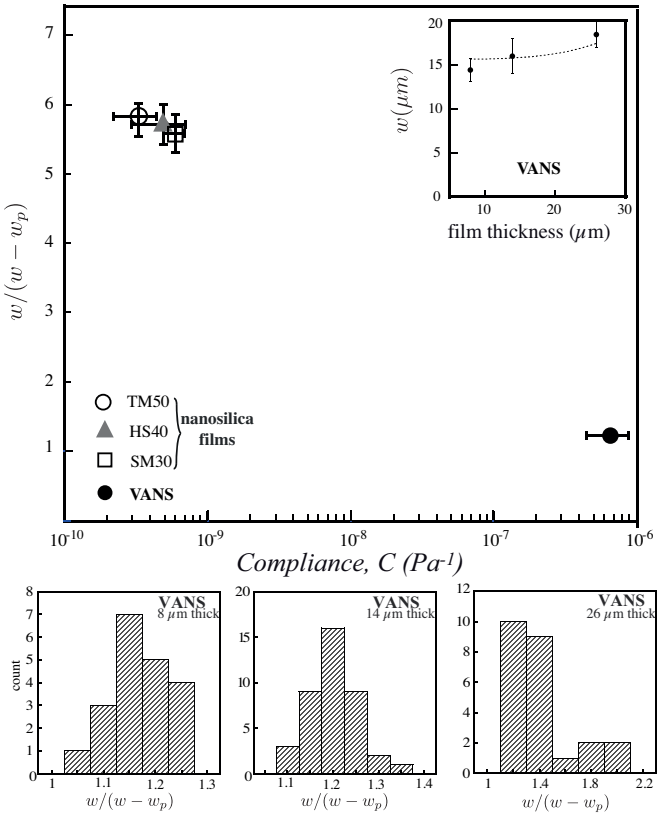

FIG. 10. Ratio between the crack opening, w, and the reversible part, $w-w_p$, of the crack displacement as a function of the film compliance, $C=E^{-1}$, in semi-log scale. Nanosilica films are obtained by the drying of aqueous suspensions of silica particles whose size is 7nm (Ludox SM30), 12nm (Ludox HS40) and 22nm (Ludox TM50). Inset: mean crack opening vs. film thickness (the dashed line is the best fit by equation 6). Statistics on $w/(w-w_p)$ for nanospring films of various thicknesses: the mean value is 1.16 ± 0.06, 1.20 ± 0.05, and 1.37 ± 0.23 for 8μm thick, 14μm and 26μm thick, respectively. The black dot in the graph combines these different mean values.

films the following events can be outlined: changes in the microstructures, the modification of the bonds between nanosprings, plastic deformation of nanosprings beyond their yield strength as observed or irreversible entanglement of nanosprings induced par the capillary shrinkage. In the case of particulate coatings, the plasticity is essentially related to changes in the microstructure. Moreover the inhomogeneity of the film should undoubtedly affect the crack healing even if the homogeneity of the nanospring films was not quantified in the present study.

Finally, the crack opening and closing in nanosprings films are remarkably reproducible with subsequent wetting-drying cycles. In this way, a drop of a low-surface-tension solvent is imbibed in a nanospring film then crack formation is induced by the drying process. The same process is repeated several times and the crack opening/closing is measured. The high repeatability of the crack opening/closing is demonstrated in figure 11. Here, the duration between two successive cycles is chosen so that the drying process is complete between each

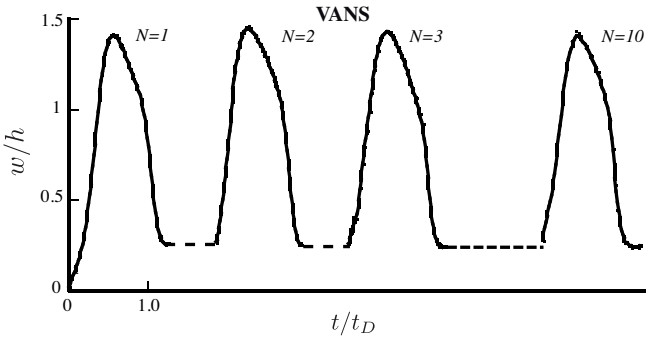

FIG. 11. Measurements of the crack opening and closing of a nanosprings film during successive wetting/drying processes ($N=10$ cycles); the measurements are performed on the same crack.

cycle; hence, the film of nanosprings becomes dry between each cycle. This behaviour can be associated with the mechanical stability of nanospring films under repeated loading tests as shown in section II B 1.

IV. CONCLUSION

Nanostructured layers made of Vertically-Aligned NanoSprings, e.g. VANS, are both dense and highly porous materials. Moreover, the high compliance of these films when compared to conventional coatings have been highlighted through nanoindentation testing. Under wetting/drying processes the film cracks. The resulting crack patterns are similar to those usually observed. However, in the case of VANS the cracks partially close when the drying process ceases. Based on considerations related to the scale of the film as well as the scale of the individual nanosprings, we have shown that this quasi-healing is associated with the compliance, the weak plasticity and the high deformability of the individual nanosprings that form the film. Moreover, the mechanical stability of the films has been highlighted through cyclic loading and repeated wetting/drying processes.

V. SUPPLEMENTARY MATERIAL

See supplementary material for multicyclic indentation results.

ACKNOWLEDGMENTS

The authors thank Aurore Sibrant for fruitful discussions. This work has benefited from a French State grant 'BOGUS' ANR-19-CE06-0030-02 and the US Office of Naval Research (Grant #: N00014-20-1-2433).

DATA AVAILABILITY STATEMENT

AIP Publishing believes that all datasets underlying the conclusions of the paper should be available to readers. Authors are encouraged to deposit their datasets in publicly available repositories or present them in the main manuscript. All research articles must include a data availability statement stating where the data can be found. In this section, authors should add the respective statement from the chart below based on the availability of data in their paper.

[1] N. I. Kovtyukhova, B. R. Martin, J. K. N. Mbindyo, P. A. Smith, B. Razavi, T. S. Mayer, and T. E. Mallouk, "Layer-by-layer assembly of rectifying junctions in and on metal nanowires," The Journal of Physical Chemistry B **105**, 8762–8769 (2001).

[2] P. Bakharev, V. Dobrokhotov, and D. McIlroy, "A method for integrating zno coated nanosprings into a low cost redox-based chemical sensor and catalytic tool for determining gas phase reaction kinetics," Chemosensors **2**, 56–68 (2014).

[3] X. Duan, J. Wang, and C. M. Lieber, "Synthesis and optical properties of gallium arsenide nanowires," Applied Physics Letters **76**, 1116–1118 (2000), https://doi.org/10.1063/1.125956.

[4] Z. Tang, N. A. Kotov, and M. Giersig, "Spontaneous organization of single cdte nanoparticles into luminescent nanowires." Science **297**, 237–240 (2002).

[5] D. McIlroy, D. Zhang, Y. Kranovand, and M. Norton, "Nanosprings," Appl.Phys.Lett. **79**, 1540 – 1542 (2001).

[6] L. Wang, D. Major, P. Paga, D. Zhang, M. G. Norton, and D. N. McIlroy, "High yield synthesis and lithography of silica-based nanospring mats," Nanotechnology **17**, S298–S303 (2006).

[7] Z. Xia and J. Hutchinson, "Crack patterns in thin films," Journal of the Mechanics and Physics of Solids **48**, 1107 – 1131 (2000).

[8] P. Bacchin, D. Brutin, A. Davaille, E. Di Giuseppe, X. D. Chen, I. Gergianakis, F. Giorgiutti-Dauphiné, L. Goehring, Y. Hallez, R. Heyd, R. Jeantet, C. Le Floch-Fouéré, M. Meireles, E. Mittelstaedt, C. Nicloux, L. Pauchard, and M.-L. Saboungi, "Drying colloidal systems: Laboratory models for a wide range of applications," The European Physical Journal E **41**, 94 (2018).

[9] S. Sadhukhan, A. Kumar, G. U. Kulkarni, S. Tarafdar, and T. Dutta, "A spring network simulation in three dimensions for designing optimal crack pattern template to fabricate transparent conducting electrodes," Bulletin of Materials Science **42**, 197 (2019).

[10] J. Walker, "Cracks in a surface look intricately random but actually develop rather systematically," Scientific American **255**, 178 – 183 (1986).

[11] C. Brinker and G. Scherer, *Sol-Gel Science: The Physics and Chemistry of Sol-Gel Processing* (Academic Press: New York, 1990).

[12] A. Atkinson and R. Guppy, "Mechanical stability of sol-gel films," Journal of Materials Science **26**, 3869 – 3873 (1991).

[13] A. Groisman and E. Kaplan, "An experimental study of cracking induced by desiccation," Europhys. Lett. **25**, 415 – 420 (1994).

[14] L. Goehring, W. J. Clegg, and A. F. Routh, "Plasticity and fracture in drying colloidal films," Phys. Rev. Lett. **110**, 024301 (2013).

[15] F. Giorgiutti-Dauphiné and L. Pauchard, "Painting cracks: A way to investigate the pictorial matter," Journal of Applied Physics **120**, 065107 (2016), https://doi.org/10.1063/1.4960438.

[16] D. McIlroy, A. Alkhateeb, D. Zhang, D. Aston, A. Marcy, and M. Norton, "Nanospring formation - unexpected catalyst mediated growth," J. Phys. Condens. Matter **16**, R415 – R440 (2004).

[17] Y. P. Timalsina, D. Oriero, T. Cantrell, T. Prakash, J. Branen, D. E. Aston, K. Noren, J. J. Nagler, S. Rastogi, D. N. McIlroy, and G. Corti, "Characterization of a vertically aligned silica nanospring-based sensor by alternating current impedance spectroscopy," Journal of Micromechanics and Microengineering **20**, 095005 (2010).

[18] P. M. Wojcik, P. V. Bakharev, G. Corti, and D. N. McIlroy, "Nucleation, evolution, and growth dynamics of amorphous silica nanosprings," Mater. Res. Express **4**, 015004 (2017).

[19] W. Oliver and G. Pharr, J. Mater. Res. **7**, 1564 (1992).

[20] H. Hirakata, S. Matsumoto, M. Takemura, M. Suzuki, and T. Kitamura, "Anisotropic deformation of thin films comprised of helical nanosprings," International Journal of Solids and Structures **44**, 4030 – 4038 (2007).

[21] A. F. da Fonseca and D. S. Galvão, "Mechanical properties of nanosprings," Phys. Rev. Lett. **92**, 175502 (2004).

[22] E. Di Giuseppe, A. Davaille, E. Mittelstaedt, and M. François, "Rheological and mechanical properties of silica colloids: from newtonian liquid to brittle behaviour," Rheologica Acta **51**, 451–465 (2012).

[23] L. Wang, C. Ortiz, and M. C. Boyce, "Mechanics of indentation into micro and nanoscale forests of tubes, rods, or pillars," Journal of Engineering Materials and Technology **133** (2010).

[24] H. Liu, J. Zhai, and L. Jiang, "Wetting and anti-wetting on aligned carbon nanotube films," Soft Matter **2**, 811–821 (2006).

[25] E. Washburn, Phys. Rev. **17**, 273 (1921).

[26] C. Wirth, S. Hofmann, and J. Robertson, "Surface properties of vertically aligned carbon nanotube arrays," Diamond and Related Materials **17**, 1518–1524 (2008).

[27] C. Py, R. Bastien, J. Bico, B. Roman, and A. Boudaoud, "3d aggregation of wet fibers," Europhysics Letters (EPL) **77**, 44005 (2007).

[28] S. Bohn, L. Pauchard, and Y. Couder, "Hierarchical crack pattern as formed by successive domain divisions. I. Temporal and geometrical hierarchy," Phys. Rev. E **71**, 046214 (2005).

[29] M. Leang, F. Giorgiutti-Dauphine, L.-T. Lee, and L. Pauchard, "Crack opening: from colloidal systems to paintings," Soft Matter **13**, 5802–5808 (2017).

[30] B. Lawn, *Fracture of Brittle Solids*, 2nd ed., Cambridge Solid State Science Series (Cambridge University Press, 1993).